Systemic inflammation suppresses lymphoid tissue remodeling and B cell immunity during concomitant local infection

Yannick O Alexandre[1], Sapna Devi[1,2], Simone L Park[1], Laura K. Mackay[1,2], William R. Heath[1,2], Scott N. Mueller[1,2]*

[1]Department of Microbiology and Immunology, The University of Melbourne, The Peter Doherty Institute for Infection and Immunity, Melbourne, Victoria 3000, Australia.

[2]The Australian Research Council Centre of Excellence in Advanced Molecular Imaging, The University of Melbourne, Melbourne, Victoria 3000, Australia.

* Corresponding author. Email: smue@unimelb.edu.au

Keywords: Inflammation; lymphopenia; pathogen coinfection; immune response; B cells; lymphoid stromal cells.

Abstract

Concurrent infection with multiple pathogens occurs frequently in individuals and can result in exacerbated infections and altered immunity. However, the impact of such coinfections on immune responses remains poorly understood. Here we reveal that systemic infection results in an inflammation-induced suppression of local immunity. During localized infection or vaccination in barrier tissues including the skin or respiratory tract, concurrent systemic infection induced a type I interferon-dependent lymphopenia that impairs lymphocyte recruitment to the draining lymph node (dLN). This leads to suppressed lymphoid stromal cell expansion and dLN remodeling and impaired induction of B cell responses and antibody production. Our data suggest that contemporaneous systemic inflammation constrains the induction of regional immunity.

Introduction

Viral pathogens that infect the skin and mucosa, including herpes simplex virus (HSV) and influenza viruses, induce immune responses in lymph nodes (LN) that drain the site of local infection. Although immune responses to infection with a single pathogen are well defined, people are often infected with multiple pathogens simultaneously and such pathogen coinfections can impair immune responses and alter the outcomes of infections (Mabbott, 2018; Stelekati and Wherry, 2012). Moreover, systemic pathogen infections including HIV, malaria, COVID-19 and bacterial sepsis, as well as other diseases including autoimmune disorders and stroke, result in systemic inflammation that can lead to immunosuppression. Such systemic infections or inflammatory responses are often correlated with reduced protection against localized coinfections (Chang et al., 2013; Edwards et al., 2015; Hotchkiss et al., 2013; Langhorne et al., 2000). Yet, the mechanisms underlying altered immunity during coinfection or inflammation remain poorly understood.

The induction of immune responses relies upon effective recruitment of B cells and T cells from the circulation where they can encounter cognate viral antigens presented by professional antigen presenting cells. Coordinated cellular interactions define T and B cell activation, proliferation and differentiation, and these interactions are supported by specialized microanatomical compartments within LNs (Alexandre and Mueller, 2018). Networks of non-hematopoietic lymphoid stromal cells (LSCs) construct the microarchitecture of LNs, providing both structural and functional support for the induction of immune responses. Lymphatic endothelial cells (LEC) form the afferent and efferent lymphatic vessels required for sampling peripheral tissues and exit of lymphocytes back to the blood circulation, respectively. Lymphocytes that enter the LN from the blood are recruited via specialized blood endothelial cells (BEC) that form PNAd^{+} high endothelial venules (HEV) (Mueller and Germain, 2009). Subsets of mesenchymal fibroblastic reticular cells (FRC) construct the LN architecture and include marginal reticular cells (MRC), follicular dendritic cells (FDC), T cell zone FRC and additional reticular cells localized in B cell follicles. FRC are identified on the basis of expression of podoplanin (PDPN; also called gp38) and lack expression of the endothelial cell marker CD31. FRC respond dynamically to inflammation by modulating their gene expression program that influences immune responses (Gregory et al., 2017; Malhotra et al., 2012). This includes down-regulation of the expression of the chemokines CCL19 and CCL21, which affects the positioning of CD8 and CD4 T cells (Mueller et al., 2007a). The

importance of the mesenchymal LSC network was demonstrated in studies showing that depletion of the FRC network results in impaired induction of immune responses (Cremasco et al., 2014; Denton et al., 2014).

Localized infections induce considerable enlargement of the draining LNs to facilitate immune responses, including recruitment and proliferation of lymphocytes and expansion of stromal cell networks. T cell responses are initiated rapidly within LNs, with activation and proliferation of pathogen-specific T cells occurring in as little as 2 days, followed by egress of the expanded pool of effector cells after 5-6 days. B cell responses are initiated with similar rapidity, and B cells differentiate into short-lived antibody secreting cells (ASC) within days, while other B cells migrate to B cell follicles to form germinal centers (GC) and differentiate into high affinity plasma blasts (PB) or memory B cells. GCs form within days after infection and can persist for weeks or months. LN expansion peaks 1-2 weeks after infection, which is delayed relative to the induction of T cell responses, suggesting that remodeling of LN stromal cell networks may be particularly important for supporting B cell responses. We have previously shown that LN remodeling after HSV infection requires recruitment of lymphocytes from the circulation to induce LN expansion, while B cells can sustain stromal cell responses (Gregory et al., 2017).

Here, we examined the impact of systemic infection on an ongoing local immune response. We show that the induction of systemic inflammation in response to coinfection of mice with lymphocytic choriomeningitis virus (LCMV) or Toll-like receptor (TLR) agonists impaired LN swelling and stromal cell remodeling and inhibited B cell responses to localized infection or vaccination. Systemic inflammation induced a type I interferon (IFN-I) dependent lymphopenia, impairing the recruitment of B cells to draining LNs and hindering the induction of humoral immune responses. Our findings reveal that a consequence of an acute systemic inflammatory response is the suppression of the ability to induce local immunity.

98 **Results**

99 *Restrained LN remodeling and suppressed B cell responses after LCMV infection.*

100 We first investigated how different viral pathogens influence lymphoid tissue remodeling. We
101 infected mice subcutaneously in the footpad with HSV or LCMV Armstrong and enumerated
102 stromal cell populations in the draining popliteal LN (pLN) by flow cytometry 8 days after
103 infection (Fig. 1A). HSV inoculation results in an infection that remains localized to tissues
104 near the site of inoculation (Gregory et al., 2017), whereas LCMV replicates locally as well as
105 spreading systemically, including to the spleen (Jones et al., 2000; Olson et al., 2012). HSV
106 infection induced a marked increase in total pLN cellularity and expanded all populations of
107 pLN LSC: PDPN$^+$ FRC, PDPN$^+$ CD31$^+$ LEC, CD31$^+$ BEC and CD31$^+$ PNAd$^+$ HEV (Fig. 1B).
108 In contrast, LCMV infection resulted in only a marginal increase in cellularity and no
109 significant expansion of the subsets of LSC in the LN compared to uninfected mice (Fig. 1B).

110 Examination of pLN by confocal microscopy revealed substantial enlargement of the draining
111 LN after HSV infection, whereas pLN were small and lacked organized B cell zones after
112 LCMV infection (Fig. 1C). Closer examination revealed substantial disorganization of the
113 PDPN$^+$ T cell zone FRC network that ensheaths laminin$^+$ reticular fibers (Fig. 1D) and loss of
114 B cell zone stromal cell organization after LCMV infection (Fig. 1E). Notably, in LCMV
115 infected mice B cell follicles were highly disorganized, and we could not detect FDC, whereas
116 B cell follicle organization and FDCs were intact in HSV infected mice (Fig. 1E). Moreover,
117 we observed the formation of a network of PDPN$^+$ FRC on the capsular side of the B cell
118 follicles in LCMV infected mice (Fig. 1E, yellow arrows). This indicated that the B cell
119 follicles retracted from the LN capsule and a population of subcapsular PDPN$^+$ FRC formed in
120 this zone during LCMV infection.

121 Because MAdCAM-1$^+$ MRC form a specialized stromal layer between B cell follicles and the
122 subcapsular sinus, we postulated that the expanded subcapsular LSC in LCMV infected mice
123 might be MRC, but subsequent analysis revealed that MAdCAM-1$^+$ were not expanded
124 following LCMV infection. Conversely, we observed a substantial increase in MAdCAM-1$^+$
125 PDPN$^+$ FRC after HSV infection (Fig. 1F). Greater than half of all FRC were MAdCAM-1$^+$
126 after HSV infection (Fig. 1G), suggesting that expression of this adhesion molecule was
127 upregulated after HSV but not LCMV infection. Staining of tissue sections confirmed
128 increased expression of MAdCAM-1 on T cell zone FRC in pLN after HSV but not LCMV

infection (Fig. S1). This suggests that MAdCAM-1, which is typically used to define MRC and is also expressed by FDC in LNs, is not a reliable marker of MRC after infection.

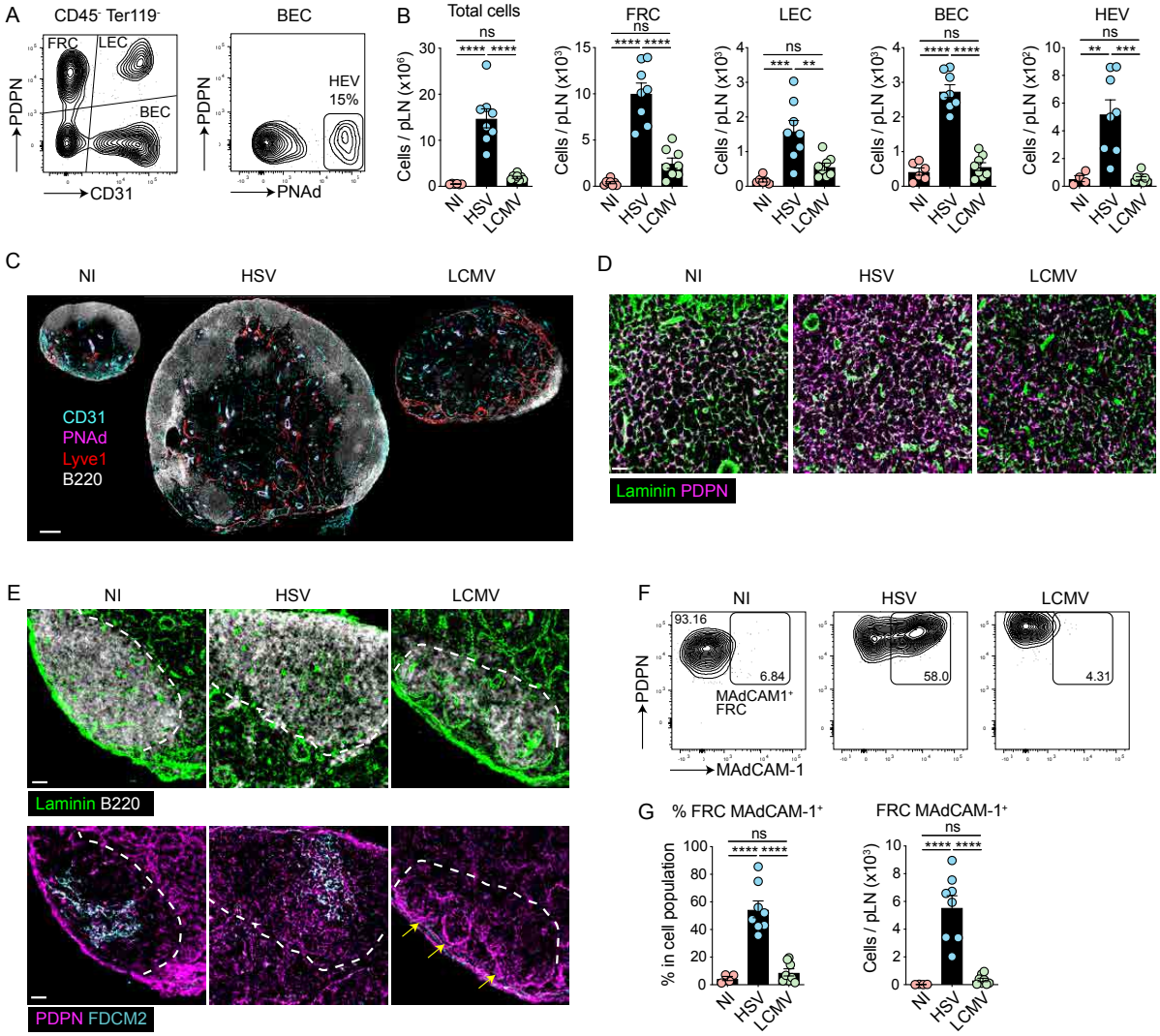

Fig. 1. Restrained remodeling of the draining LN during LCMV infection. (A) Gating strategy to identify CD45$^-$ Ter119$^-$ stromal cell subsets by flow cytometry. (B) Numbers of total cells and stromal cell subsets in the pLN from uninfected (NI) mice and mice infected s.c. with HSV or LCMV analyzed by flow cytometry. Graphs show pooled data (mean ± SEM) from 3 independent experiments each with 2-3 mice per group. *P < 0.05, **P < 0.01, *** P < 0.001, ****P < 0.0001, ns, non-significant, by ANOVA with Tukey's multiple comparisons test. (C-E) pLN sections from NI, HSV or LCMV infected mice were stained for B220, Lyve1, CD31 and PNAd (C), laminin and podoplanin (D) or laminin, B220, podoplanin, amd FDC-M2 (E) and analyzed by confocal microscopy. Data are representative of 2 experiments with 3 mice per group. Dotted lines depict border of B cell follicles and arrows show subcapsular FRC in LCMV pLN that were not observed in NI or HSV pLN. Scale bars, 200µm (C), 30µm (D-E) (F) MAdCAM-1 expression on FRC from NI mice and following HSV or LCMV infection. (G) Percentage and numbers of MAdCAM-1$^+$ FRC in the pLN of NI and mice infected s.c. with HSV or LCMV. Graphs show pooled data (mean ± SEM) from 3 independent experiments each with 2-3 mice per group. ****P < 0.0001, ns, non-significant, by ANOVA with Tukey's multiple comparisons test.

Next, we examined virus-specific CD8$^+$ T cell responses in the pLN by major histocompatibility complex class I (MHC-I) tetramer staining. Local infection with LCMV induced larger numbers of virus-specific CD8$^+$ T cells compared to HSV infection (Fig. 2A-B). In contrast, we found that B cell numbers were significantly reduced in draining pLN after LCMV infection in comparison with HSV infected mice (Fig. 2D). Expansion of GL7$^+$ germinal center (GC) B cells and CD138$^+$ antibody secreting cells (ASC) was also significantly lower in the pLN after LCMV infection compared to HSV infection (Fig. 2C-E). B cell follicles were increased in size after HSV infection and contained GL7$^+$ GC B cells, while B cell follicles were markedly reduced in size and GL7$^+$ cells were extrafollicular in LCMV infected mice (Fig. 2F). Large numbers of CD138$^+$ ASC accumulated at the border between T and B cell zones and within the medullary cords after HSV infection, whereas ASC were reduced and only observed in the medulla during LCMV infection (Fig. 2F). Thus, LCMV infection results in diminished LN remodeling, loss of B cell follicles and restrained B cell responses in draining LN.

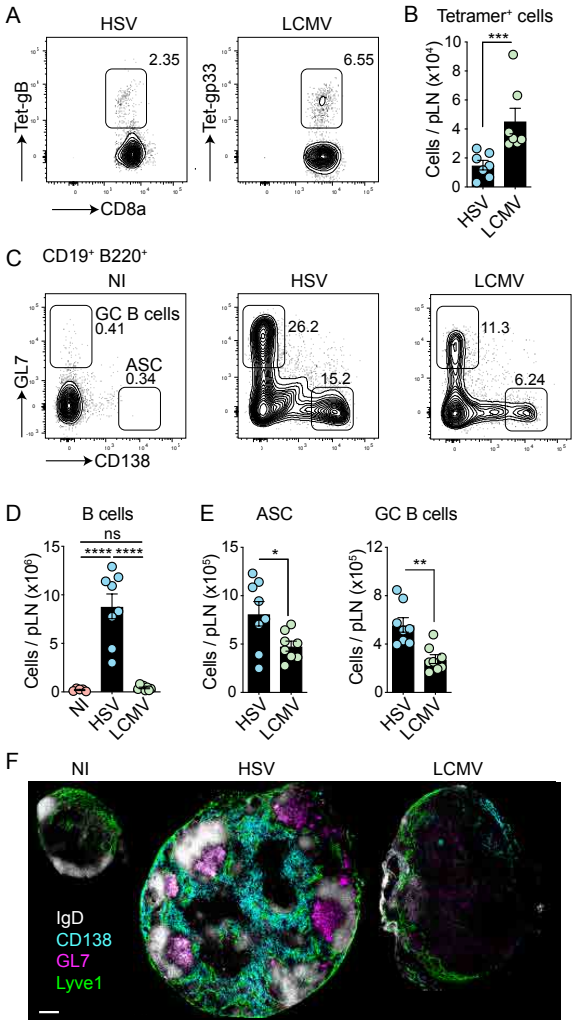

163 **Fig. 2. Suppressed B cell responses during LCMV infection.** (A) Tetramer staining of $CD8^+$
164 T cells, following HSV and LCMV infection. (B) Numbers of $CD8^+$ $Tetramer^+$ cells in the pLN
165 of HSV and LCMV-infected mice. Data are pooled from 2 independent experiments with 3-4
166 mice per group. ***P < 0.001, by Mann-Whitney test. (C) Flow cytometry analysis of $GL7^+$
167 GC B cells and $CD138^+$ ASC. B cells were first gated on live $CD19^+$ $CD3^-$ $NK1.1^-$ cells. (D)
168 Absolute numbers of B cells in the popliteal LN from NI mice and mice infected with HSV or
169 LCMV. Graphs show pooled data (mean ± SEM) from 3 independent experiments each with
170 2-3 mice per group. ****P < 0.0001, ns, non-significant, by ANOVA with Tukey's multiple
171 comparisons test. (E) ASC and GC B cells in the pLN from mice infected with HSV or LCMV.
172 Graphs show pooled data (mean ± SEM) from 2 independent experiments each with 4 mice
173 per group. *P < 0.05, **P < 0.01, by unpaired two-tailed t test. (F) pLN sections from NI, HSV
174 or LCMV infected mice were stained for IgD, CD138, GL7 and Lyve1 and analyzed by
175 confocal microscopy. Data are representative of 2 experiments with 3 mice per group. Scale
176 bar, 200μm.
177

178 *LCMV coinfection suppresses LN remodeling in response to localized infection.*

179 The subdued stromal cell expansion and altered lymphoid tissue architecture observed
180 following LCMV infection led us to investigate the impact of LCMV infection on LN
181 remodeling during localized HSV coinfection. We infected mice with HSV in the footpad and
182 coinfected the mice 2 days later with LCMV either by the same route or systemically by
183 intraperitoneal infection (Fig. 3A). LCMV coinfection by either route markedly restrained the
184 increase in pLN cellularity induced by HSV infection and suppressed FRC expansion (Fig.
185 3B). Local infection with LCMV resulted in infection of pLN FRC whereas systemic LCMV
186 infection did not (Fig. S2A). Yet, both routes of infection resulted in equivalent suppression of
187 the draining LN response (Fig. 3B), ruling out an inhibitory role of LCMV through direct
188 infection of FRC. Since local LCMV infection also results in systemic spread of virus from the
189 LN to spleen (Olson et al., 2012), we performed subsequent experiments using systemic LCMV
190 coinfection. Importantly, LCMV coinfection did not alter the growth of HSV in the tissue (Fig.
191 3C).

192 We examined HSV-draining pLN sections by confocal microscopy and discovered that LCMV
193 coinfection prominently altered pLN remodeling in response to HSV. In coinfected mice, B
194 cell follicles were small and disorganized and LYVE-1^+ medullary sinuses were more
195 prominent compared to mice infected with HSV alone (Fig. 3D). Closer examination of B cell
196 follicles in coinfected mice revealed fewer B cells, reduction of the FDC network within the
197 follicles and recession of the follicles away from the pLN subcapsular sinus (Fig. 3E).
198 Strikingly, a dense network of $PDPN^+$ FRC formed between B cell follicles and the pLN

199 capsule in coinfected mice (Fig. 3E, yellow arrows), similar to what we observed during local
200 LCMV infection (Fig. 1E), that was absent from mice infected with HSV alone.

201 Quantification of cells by flow cytometry revealed a significant reduction in total cellularity
202 and reduced expansion of pLN FRC, LEC, BEC and PNAd^{+} HEV in HSV-draining LN from
203 LCMV coinfected mice (Fig. 3F). Coinfection suppressed the induction of MAdCAM-1 on
204 FRC (Fig. 3G), resulting in a significant reduction in both MAdCAM-1^{+} as well as MAdCAM-
205 1^{-} FRC (Fig. S2B). We also examined CD157 (BP-3) expression on FRC, a marker that has
206 been used to identify subpopulations of FRC including CD157-lo medullary FRC (Huang et
207 al., 2018). Both CD157^{+} T cell zone FRC and CD157-lo medullary FRC populations were
208 reduced in the pLN of mice coinfected with HSV and LCMV in comparison with mice infected
209 with HSV alone (Fig. 3H).

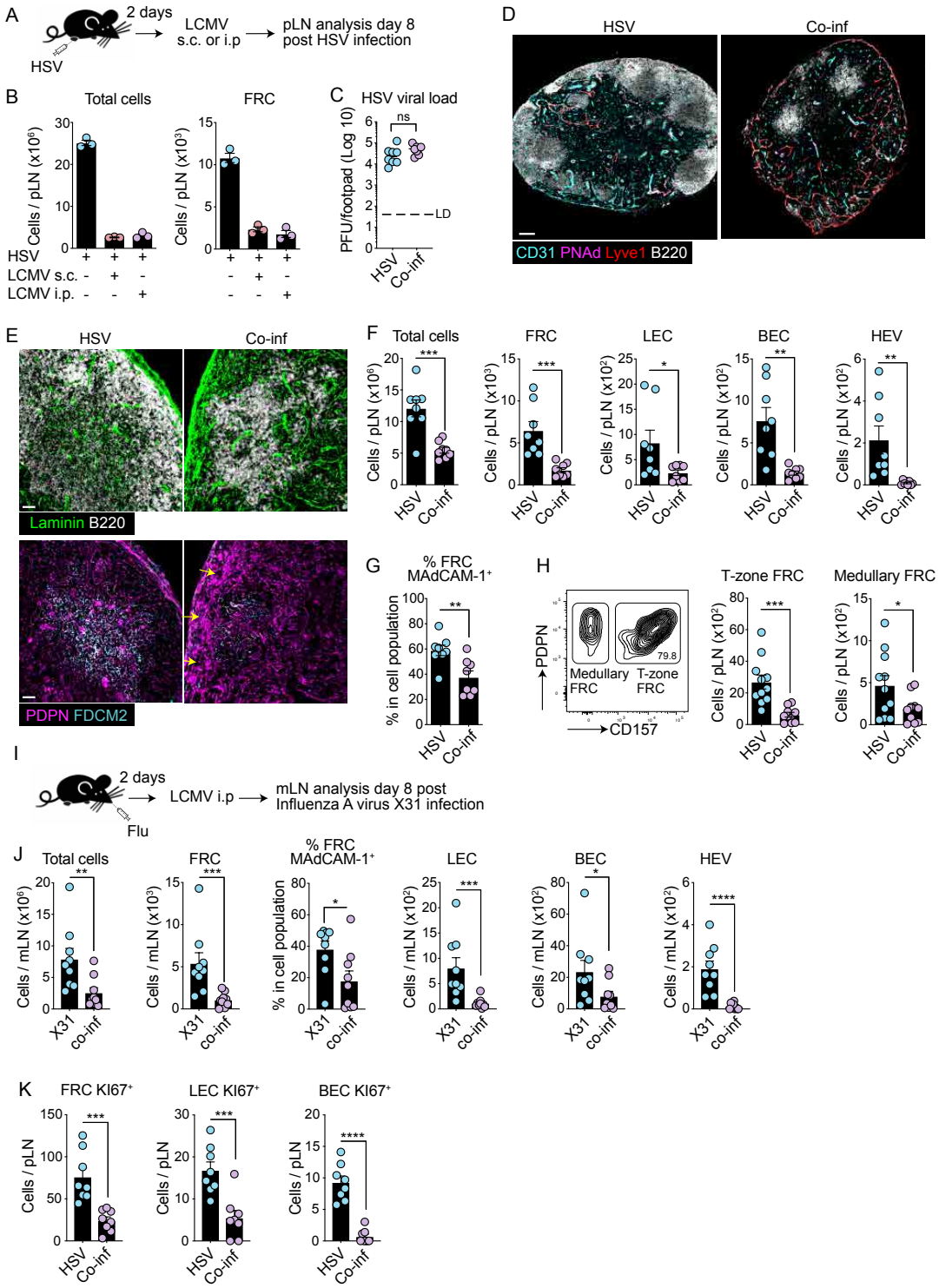

Fig. 3. LCMV coinfection suppresses lymphadenopathy to localized infection. (A) Experimental schematic of coinfection. Mice were infected subcutaneously (s.c.) with HSV and 2 d later infected with LCMV s.c. or intraperitoneally (i.p.). pLN were analyzed 8 d post HSV infection. (B) Numbers of total cells and FRC in the pLN of infected mice analyzed by flow cytometry. Graphs are representative of 2 experiments with 2-3 mice per group (mean ± SEM). (C) HSV viral load in the footpad of infected mice. Mice were infected as in A and footpad tissue harvested 5 d post-HSV infection for plaque assay. Data are pooled from 2 independent experiments with 4 mice per group. ns, non-significant, by Mann-Whitney test LD: limit of detection. (D-E) pLN sections from NI, HSV or coinfected mice were stained for B220, Lyve1, CD31, and PNAd (D), Laminin, B220, podoplanin, and FDC-M2 (E) and

221 analyzed by confocal microscopy. Data are representative of 2 experiments with 3 mice per
222 group. Scale bar, 40µm. (F-G) Numbers of total cells and stromal cell subsets (F) and
223 MAdCAM-1 expression analysis on FRC (G) in the pLN of HSV and coinfected mice analyzed
224 by flow cytometry. Graphs show pooled data (mean ± SEM) from 2 independent experiments
225 with 4 mice per group. (H) Expression of CD157 on PDPN$^+$ CD31$^-$ MAdCAM-1$^-$ CD21/35$^-$
226 cells to define T cell zone FRC (CD157$^+$) and medullary FRC (CD157$^-$) by flow cytometry.
227 Graphs are pooled data of 3 experiments with 2-4 mice per group (mean ± SEM). *P < 0.05,
228 **P < 0.01, *** P < 0.001, ****P < 0.0001, by unpaired two-tailed t test (F-H). (I) Mice were
229 infected intranasally with Flu-gB and 2 d later infected systemically with LCMV. Mediastinal
230 LN (medLN) were analyzed 8 d post Flu infection. (J) Numbers of total cells, stromal cell
231 subsets, and MAdCAM-1 expression analysis on FRC in the medLN of Flu and coinfected
232 mice analyzed by flow cytometry. Graphs show pooled data (mean ± SEM) from 2 independent
233 experiments with 4-5 mice per group. *P < 0.05, **P < 0.01, *** P < 0.001, ****P < 0.0001,
234 by Mann-Whitney test. (K) Ki67$^+$ stromal cell subsets following HSV and coinfection. Mice
235 were infected as in A and pLN harvested 5 d post-HSV infection and intracellular KI67
236 expression was analyzed flow cytometry. Graphs show pooled data (mean ± SEM) from 2
237 independent experiments each with 4 mice per group. *** P < 0.001, ****P < 0.0001, by
238 unpaired two-tailed t test.
239

240 These data suggested that LCMV coinfection inhibited LN expansion in response to local HSV
241 infection. To determine if systemic coinfection also suppressed dLN responses to other
242 localized infections, we infected mice intranasally with Influenza A virus X31 and coinfected
243 these mice with LCMV 2 days later (Fig. 3I). Coinfection suppressed immune responses in the
244 draining mediastinal LNs (mLN), resulting in reduced cellularity and impaired expansion of
245 FRC, LEC, BEC and PNAd$^+$ HEV, as well as impaired upregulation of MAdCAM-1 by mLN
246 FRC compared to mice infected with influenza alone (Fig. 3J). This indicated that systemic
247 infection concurrent with either a skin or respiratory viral infection suppresses immune
248 responses in the LN draining the site of localized challenge.

249 Since systemic coinfection suppressed expansion of pLN LSC, we wanted to know if this was
250 due to reduced proliferation or altered survival of LSC. We examined proliferating LSC in
251 LCMV and HSV coinfected mice by staining for Ki67. Significantly fewer Ki67$^+$ FRC, LEC
252 and BEC were detected in coinfected mice when compared to mice infected with HSV alone
253 (Fig. 3K). In contrast, coinfection did not alter the number of apoptotic (Annexin-V+ PI+)
254 FRC, LEC or BEC compared to that observed following infection with HSV alone (Fig. S2C).
255 Further, we observed no alterations in metabolic functions as determined by glucose or lipid
256 uptake, mitochondrial mass or oxidative stress in pLN LSC in coinfected mice compared to
257 mice infected with HSV alone (Fig. S2D-E). Thus, systemic LCMV coinfection suppressed
258 dLN remodeling and stromal cell expansion in response to localized infection.

259

260 *Systemic coinfection suppresses B cell responses to localized infection*

261 We examined immune responses in HSV and LCMV coinfected mice and observed that
262 although total numbers of $CD8^+$ T cells in the pLN were reduced by coinfection, HSV-specific
263 $CD8^+$ T cell responses were unaffected (Fig. 4A). Systemic LCMV coinfection also reduced
264 the accumulation of total $CD4^+$ T cells in the draining pLN and suppressed the induction of T
265 follicular helper (T_{FH}) cells compared to mice infected with HSV alone (Fig. 4B, S3A). B cell
266 numbers were significantly reduced in the pLN of coinfected mice and the induction of GC B
267 cells and ASCs was impaired (Fig. 4C). This suppression of local B cell responses during
268 LCMV coinfection was not due to increased apoptosis of B cells or T cells, as indicated by
269 AnnexinV staining (Fig. 4D). Histological examination of pLN sections revealed a reduction
270 in the size and numbers of $GL7^+$ GC B cells and fewer $CD138^+$ plasma cells in coinfected mice
271 (Fig. 4E). Moreover, systemic LCMV coinfection significantly suppressed HSV-specific
272 antibody responses (Fig. 4F).

273 To further investigate the impact of systemic coinfection on the induction of local antigen-
274 specific B cell responses, we examined ovalbumin (OVA)-specific B cell receptor transgenic
275 OB-I B cell responses following transfer into B6 mice and immunization with OVA in
276 complete freunds adjuvant (OVA/CFA) (Fig, 4G). OB-I B cells expanded significantly in the
277 pLN following sub-cutaneous OVA/CFA immunization and formed GC B cells and ASCs (Fig.
278 4H and Fig S3B). Coinfection of mice with LCMV significantly impaired the expansion of the
279 OB-I B cells in the pLN, reduced the number of GC cells and ASCs and reduced the frequency
280 of OB-I B cells that developed into GC cells and ASCs (Fig. 4H and Fig. S3B). Together, these
281 data show that systemic coinfection with an unrelated pathogen suppresses the induction of
282 antigen-specific B cell responses in LN draining the site of a localized challenge.

283

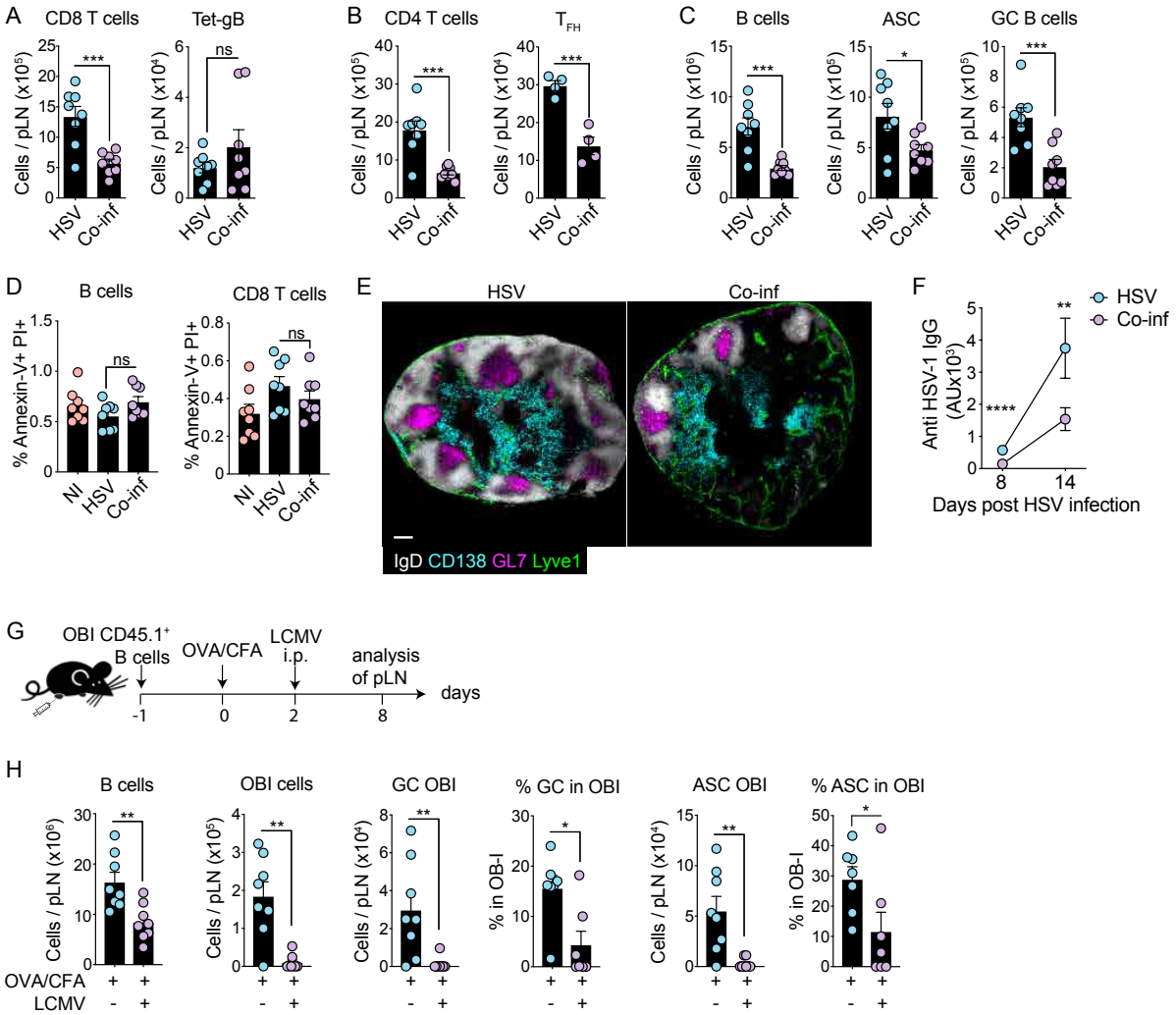

Fig. 4. Systemic coinfection suppresses B cell responses to localized infection. (A-C) Mice were infected as in Fig. 3A and pLN analyzed for CD8$^+$ T cells and HSV gB tetramer$^+$ cells (A), CD4$^+$ T cells and CXCR5$^+$ PD1$^+$ CD4$^+$ T_{FH} cells (B) and B cells (C). Graphs show pooled data (mean ± SEM) from 1-2 independent experiments with 4 mice per group. *P < 0.05, *** P < 0.001, ****P < 0.0001, ns, non-significant, by unpaired two-tailed t test. (D) Coinfection does not increase lymphocyte cell death. pLN from HSV and coinfected mice were harvested 5 d post-infection and analyzed for Annexin V and PI expression on B and CD8$^+$ T cells by flow cytometry. Inguinal LN from naïve mice were included as controls. Graphs show pooled data (mean ± SEM) from 2 independent experiments with 4 mice per group. ns, non-significant, by ns, non-significant, by unpaired two-tailed t test (E) pLN sections from NI, HSV or LCMV infected mice were stained for IgD, CD138, GL7 and Lyve1 and analyzed by confocal microscopy. Data are representative of 2 experiments with 3 mice per group. Scale bar, 200µm. (F) Serum anti–HSV-1 IgG titer assessed by ELISA. Mice were infected as in Fig. 3 and sera harvested at day 8 and 14 post-HSV infection. Graph shows pooled data (mean ± SEM) from 2 independent experiments with 4 mice per group. *P < 0.05, ** P < 0.01, by unpaired two-tailed t test. (G) Experimental schematic. Mice were given CD45.1$^+$ OBI B cells 1 day prior to footpad immunization with OVA/CFA. Mice were infected with LCMV i.p. 2 days later. pLN were analyzed 8 d. (H) OBI B cell response in the pLN. Mice were injected i.v. with transgenic OBI-GFP cells and two days later injected s.c. with an emulsion of OVA/CFA. Mice were infected i.p. with LCMV 2 d post immunization and pLN harvested 8 d post OVA/CFA injection. Graphs show pooled data (mean ± SEM) from 2 independent experiments with 4 mice per group. *P < 0.05, ** P < 0.01, by Mann-Whitney test.

307 *Coinfection-induced lymphopenia suppresses LN expansion and B cell responses*

308 CTL can kill virus infected stromal cells and B cells during infection of mice with strains of
309 LCMV that cause chronic infection (Moseman et al., 2016; Mueller et al., 2007b). To
310 determine if $CD8^+$ T cells contributed to reduced LN expansion and B cell responses during
311 coinfection with LCMV Armstrong, which is an acute infection, we infected mice with HSV
312 then treated with depleting anti-CD8α antibody prior to LCMV coinfection (Fig. 5A).
313 Suppression of pLN remodeling and impairment of B cell responses in LCMV coinfected mice
314 was unaffected by the loss of $CD8^+$ T cells (Fig. 5B and Fig. S3C). Inflammatory monocytes
315 can impair B cell responses during chronic LCMV infection (Sammicheli et al., 2016), but B
316 cell responses remained constrained with LCMV coinfection in $CCR2^{-/-}$ hosts with defective
317 recruitment of monocytes (Fig. S3D).

318 The reduction in B and T lymphocytes in the pLN of LCMV coinfected mice led us to
319 hypothesize that LCMV infection induces a general lymphopenia that traps lymphocytes in
320 distal tissues and inhibits lymphocyte recruitment to the draining LN during peripheral viral
321 infection. To examine this, we treated HSV-infected mice with the immunomodulatory drug
322 FTY720 to induce a systemic lymphopenia (Halin et al., 2005) (Fig. 5C). Expansion of pLN
323 LSC, and upregulation of MAdCAM-1 by FRC was impaired in FTY720 treated HSV infected
324 mice compared to untreated controls (Fig. 5D). B cell accumulation and induction of GC B
325 cells and ASC was also inhibited in FTY720 treated mice, whereas virus-specific $CD8^+$ T cell
326 responses were unchanged, suggesting that lymphopenia impairs the induction of local B cell
327 responses and LN remodeling but not virus-specific $CD8^+$ T cell responses (Fig. 5E).

328 To determine if B cell recruitment was required for expansion of the LN, we treated mice with
329 an anti-CD20 antibody to deplete B cells prior to HSV infection and examined stromal cell and
330 T cell responses in B cell ablated mice (Fig. 5F and Fig. S3E). In the absence of B cells, FRC
331 expansion was significantly reduced and upregulation of MAdCAM-1 by FRC was blunted,
332 whereas LEC and BEC expansion was unaffected (Fig. 5G). T cell recruitment to the HSV-
333 draining pLN and induction of HSV-specific $CD8^+$ T cell responses were unimpaired by
334 depletion of B cells (Fig. 5H). Thus, recruitment of B cells to the dLN during localized viral
335 infection is required to drive FRC expansion, while additional signals contribute to the
336 remodeling of LN endothelial cell compartments.

337 To examine if systemic coinfection impaired cell recruitment to the dLN, we adoptively
338 transferred naïve lymphocytes into HSV and LCMV coinfected mice (Fig. 5I). B cell and T

339 cell recruitment to the draining LN was suppressed, with a concomitant increase in cell
340 recruitment to distal LNs (Fig. 5J). Together, these data show that systemic coinfection impairs
341 lymphocyte recruitment to regional dLN and impairs local LN remodeling.

342

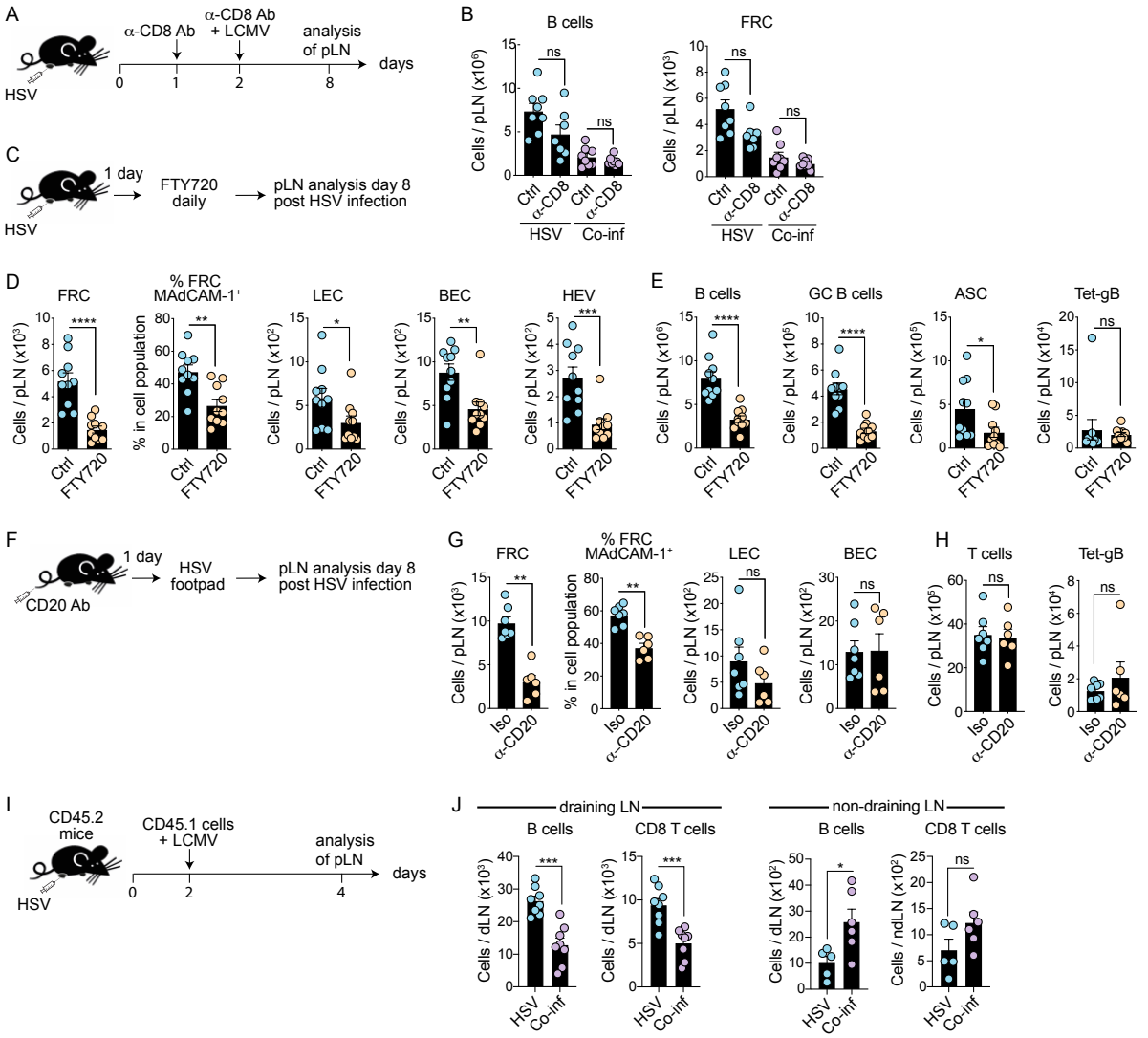

343
344 **Figure 5. Lymphopenia induced during systemic infection suppresses local LN responses.**
345 (A) Experimental schematic of CD8$^+$ T cell depletion during coinfection. Mice were infected
346 s.c. with HSV and injected with CD8 depleting antibody on days 1 and 2. Mice were infected
347 with LCMV on day 2. pLN were analyzed 8 d post HSV infection. (B) Numbers of B cells and
348 FRC in the pLN of mice infected with HSV or coinfected with or without CD8$^+$ T cells. Graphs
349 show pooled data (mean ± SEM) from 2 independent experiments with 3-4 mice per group. ns,
350 non-significant, by ANOVA with Krukal-Wallis test. (C) Experimental schematic of FTY720
351 treatment during HSV infection. Mice were infected s.c. with HSV and the following day
352 injected i.p. with FTY720 or control for 7 d. pLN were analyzed 8 d post-HSV infection. (D-
353 E) Absolute numbers of stromal cell subsets and MAdCAM-1 expression on FRC (D), B and
354 T cell responses (E) in pLN of HSV infected mice treated with FTY720. Graphs show pooled
355 data (mean ± SEM) from 2 independent experiments with 5 mice per group. (F) Experimental
356 schematic of B cell depletion during HSV infection. Mice were injected i.p. with CD20
357 depleting antibody and the following day infected s.c. with HSV. (G-H) Analysis of stromal

358 cells and T cells by flow cytometry in HSV-infected B cell-depleted mice. Graphs show pooled
359 data (mean ± SEM) from 2 independent experiments with 3-4 mice per group. (I-J) Adoptive
360 transfer of congenic lymphocytes into HSV infected mice on day 2 and LCMV coinfection,
361 with analysis of CD45.1^{+} cell numbers in the draining popliteal LN and non-draining LN 2
362 days later. *P < 0.05, **P < 0.01, *** P < 0.001, ****P < 0.0001, ns, non-significant, by Mann-
363 Whitney test (D-E, G-H, J).
364

365

366 *Systemic inflammation suppresses local immunity via IFN-I*

367 We hypothesized that systemic inflammation was responsible for the lymphopenia-induced
368 suppression of local LN responses. To examine this, we administered the TLR agonists
369 poly(I:C) or lipopolysaccharide (LPS) to HSV infected mice (Fig. 6A). Both inflammatory
370 mediators substantially reduced the HSV-driven increase in pLN cellularity, FRC expansion,
371 as well as B cell responses (Fig. 6B). Systemic LCMV infection induces the production of pro-
372 inflammatory cytokines, including type I interferon (IFN-I) (Doughty et al., 2001). LCMV
373 induced a substantial lymphopenia in mice that was dependent on IFN-I receptor (IFNAR)
374 signaling as it did not occur in *Ifnar2*$^{-/-}$ mice (Fig. S4A). We asked whether IFNAR signals
375 contributed to reduced LN hypertrophy and B cell recruitment during coinfection. We
376 generated chimeric mice with a mixture of B cell deficient (μMT$^{-/-}$) and *Ifnar2*$^{-/-}$ BM to confine
377 the lack of IFNAR expression to B cells (Fig. S4B). However, loss of IFNAR in B cells did
378 not restore LN remodeling or B cell responses in coinfected mice (Fig. S4C). Examination of
379 reciprocal BM chimeric mice generated by reconstitution of either WT or *Ifnar2*$^{-/-}$ mice with
380 WT or *Ifnar2*$^{-/-}$ BM revealed that cells in both the hematopoietic and non-hematopoietic
381 compartments contributed to altered local LN responses via IFNAR signaling (Fig. 6C and
382 S4D-E).

383 To better define the impact of IFNAR signals on local LN responses, we administered blocking
384 antibodies against IFNAR (anti-IFNAR) to mice infected with HSV or mice coinfected with
385 LCMV in order to reduce IFNAR signals (Fig. 6D). Anti-IFNAR treatment did not
386 significantly alter responses in mice infected singly with HSV (Fig. 6E). In contrast, anti-
387 IFNAR blockade significantly enhanced the expansion of FRC, LEC, BEC and HEV in
388 coinfected mice (Fig. 6E and Fig. S4F). HSV-specific T cell responses were not altered by anti-
389 IFNAR treatment (Fig. 6F), but T and B cell recruitment, GC B cells and ASC numbers were
390 restored by anti-IFNAR treatment of coinfected mice (Fig. 6G and Fig. S4F). Microscopy
391 revealed that blocking IFNAR signals improved GC formation and CD138^{+} plasma cell

392 numbers (Fig. 6H). Together, these findings show that systemic inflammation resulted in an
393 IFNAR-dependent lymphopenia that reduced cell recruitment to LN draining the site of local
394 infection and impaired LN remodeling and humoral immunity.

395

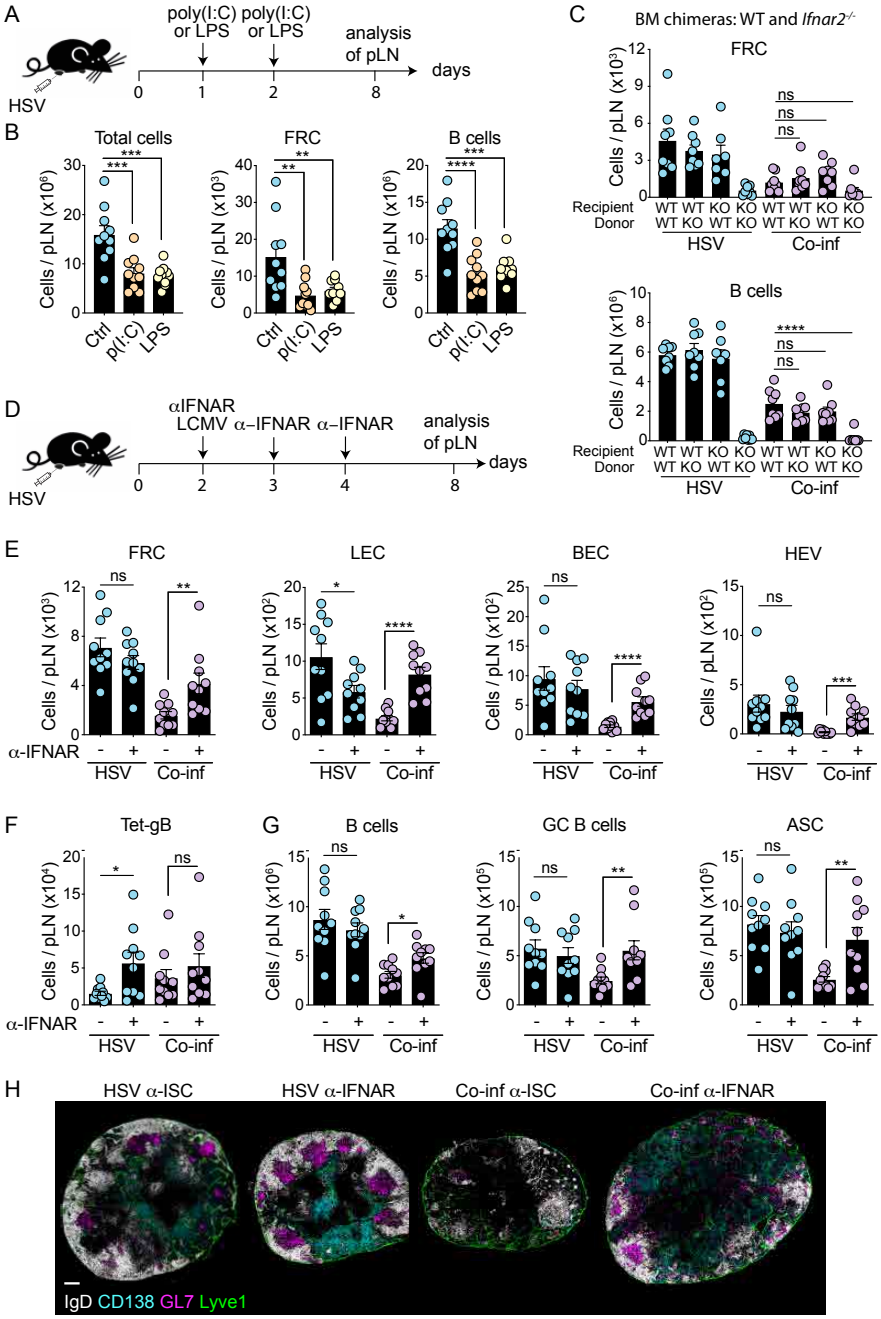

396
397 **Figure 6. Systemic inflammation suppresses local immunity via IFN-I.** (A) Experimental
398 schematic of adjuvant injection in HSV-infected mice. Mice were infected s.c. with HSV and
399 2 d later received 2 i.p. injections of either poly(I:C) or LPS 24 h apart. pLN were harvested 8
400 d post-HSV infection. (B) Numbers of total cells, FRC and B cells analyzed by flow cytometry
401 in infected mice injected with poly(I:C) or LPS. Graphs show pooled data (mean ± SEM) from
402 2 independent experiments with 5 mice per group. (C) Cell numbers in the pLN of HSV and
403 coinfected WT and *Ifnar2*$^{-/-}$ BM chimeric mice. Graphs show pooled data (mean ± SEM) from
404 two independent experiments. *P < 0.05, **P < 0.01, ***P < 0.001, ns, non-significant, by

405 ANOVA with Kruskal-Wallis test. (D) Experimental schematic of IFNAR blocking during
406 HSV and coinfection. Mice were infected s.c. with HSV, infected i.p. with LCMV on day 2
407 and injected with anti-IFNAR blocking antibody or isotype control (ISC) antibody on days 2-
408 4. Mice were analyzed on 8 d post-HSV infection. (E-G) Analysis of cellularity of stromal cell
409 subsets (E), HSV-specific $CD8^+$ T cells (F) and B cell response (G) in the pLN of HSV and
410 coinfected mice during IFNAR blocking. Graphs show pooled data (mean ± SEM) from 2
411 independent experiments with 5 mice per group. *$P < 0.05$, **$P < 0.01$, ****$P < 0.0001$, ns,
412 non-significant, by unpaired two-tailed t test (E-G). (H) pLN sections from mice treated with
413 anti-IFNAR blocking antibody or ISC were stained for IgD, CD138, GL7 and Lyve1 and
414 analyzed by confocal microscopy. Data are representative of 2 experiments with 2 mice per
415 group. Scale bar, 200μm.

416 **Discussion**

417 Coinfection with multiple pathogens occurs frequently and can alter disease outcomes and
418 subsequent immunity (Mabbott, 2018; Stelekati and Wherry, 2012). Diverse mechanisms
419 likely contribute to altered immunity during pathogen coinfections, yet our understanding of
420 these processes remains incomplete. Here, we show that widespread inflammation triggered by
421 systemic coinfection impairs dLN remodeling and B cell responses during concurrent localised
422 viral infection or immunization. Mechanistically, systemic inflammation results in an IFN-I-
423 dependent lymphopenia and impairs the recruitment of lymphocytes to LN draining sites of
424 peripheral infection, thereby constraining the induction of local humoral immunity.

425 Recruitment of lymphocytes to inflamed LNs triggers LN expansion in response to infection
426 or immunization (Gregory et al., 2017; Yang et al., 2014). This requires circulating
427 lymphocytes as a source of cells to feed the draining LN. Systemic infections (including
428 malaria and COVID-19) and autoimmune diseases (including systemic lupus erythematosus,
429 SLE) can induce lymphopenia, resulting in the trapping of lymphocytes in secondary lymphoid
430 organs around the body, thereby reducing the circulating pool of lymphocytes. We show that
431 induction of lymphopenia during systemic infection, inflammation or following FTY720
432 treatment impairs draining LN responses. B cells can coordinate the expansion of the lymphatic
433 network in LNs during inflammation (Angeli et al., 2006; Kumar et al., 2010). We show that
434 removal of B cells impaired the expansion and activation of FRC but had little impact on
435 expansion of LEC or BEC during local HSV infection. The reason for this difference is unclear
436 but may reflect the ability of both $CD4^+$ and $CD8^+$ T cells to also support LN expansion and
437 remodeling (Gregory et al., 2017).

438 Our results show that concurrent systemic inflammation impaired lymphocyte recruitment and
439 LN remodeling, which restrained B cell responses but did not impact CTL responses. LN
440 hypertrophy peaks 1-2 weeks after infection, whereas T cells are activated and leave the
441 draining LNs within 1 week (Hor et al., 2015). Conversely, B cells require a prolonged period
442 of activation and maturation within LN in order to form antibody secreting plasma cells and
443 long-lived memory B cells (Cyster and Allen, 2019). This indicates that lymphadenopathy may
444 be critical for the support of B cell responses, probably to support GC reactions and memory
445 B cell formation in the dLN. In support of this, we also observed reduced numbers of T_{FH} cells
446 in coinfected mice. Recruitment of cells to the dLN and expansion of LSC during infection
447 requires IFNAR signaling (Gregory et al., 2017). We did not find a role for direct IFNAR
448 signaling in B cells, which supports a previous study showing that $IFNAR^{-/-}$ B cells did not

449 show increased migration to LN during lymphopenia (Kamphuis et al., 2006). In contrast,
450 extrinsic IFNAR signals influence B cell accumulation in inflamed LNs (Hastey et al., 2014).
451 Whether IFNAR signaling results in the production of other inflammatory mediators (such as
452 IL-6) that further contribute to the sequestration of lymphocytes requires further investigation.

453 Many medically important pathogens cause acute or persistent systemic infections, and
454 evidence suggests that immunity to vaccination or challenge with unrelated pathogens is often
455 impaired during coinfection (Griffiths et al., 2011; Stelekati and Wherry, 2012). Models of
456 viral and bacterial coinfection have revealed increased susceptibility to infection and altered
457 responses. During the early stage of LCMV infection, IFN-I sensitizes mice to bacterial
458 endotoxin (Doughty et al., 2001; Nansen and Randrup Thomsen, 2001), which can lead to NK
459 cell-mediated impairment of the $CD8^+$ T cell responses (Straub et al., 2018). Coinfection of
460 mice with two systemic viral pathogens, LCMV and Ectromelia virus (McAfee et al., 2015) or
461 LCMV and Pichinde virus was also found to impair $CD8^+$ T cell responses to LCMV (Kenney
462 et al., 2015). In our experiments, LCMV coinfection did not inhibit HSV-specific $CD8^+$ T cell
463 responses but rather impaired the induction of local B cell responses. In humans, coinfection
464 may both directly and indirectly affect B cell differentiation and antibody production (Stelekati
465 and Wherry, 2012). Bacterial coinfection of mice with *Streptococcus pneumoniae* was shown
466 to either enhance or inhibit B cell responses to influenza virus depending on the timing of
467 respiratory coinfection (Wu et al., 2015). During the early phase of chronic LCMV infection,
468 virus-specific B cell responses can be inhibited by IFN-I production that results in death of
469 activated B cells and induction of short-lived ASCs at the expense of sustained neutralizing
470 antibody responses (Fallet et al., 2016; Moseman et al., 2016; Sammicheli et al., 2016). Other
471 viruses also directly interfere with B cell responses (Kuka and Iannacone, 2018).

472 Here, we reveal a novel mechanism by which infection can indirectly interfere with B cell
473 responses. We show that systemic inflammation induced by LCMV infection, the TLR3
474 agonist Poly(I:C) or the endotoxin LPS induced a lymphopenia that reduced the recruitment of
475 lymphocytes to the dLN during localized infection. This suppression of dLN swelling, stromal
476 cell expansion and B cell immunity suggests that opportunistic localized infections might be
477 harder to eradicate in hosts undergoing systemic inflammatory reactions. Both infectious and
478 non-infectious systemic inflammatory reactions might suppress regional immunity when
479 occurring contemporaneously. In contrast, latent coinfection with murine gammaherpesvirus
480 68 or murine cytomegalovirus was shown to protect against bacterial infection (Barton et al.,
481 2007), at least transiently (Yager et al., 2009), due to the systemic production of low levels of

482 cytokines. This indicates that the magnitude of systemic inflammation plays important roles in
483 influencing the outcomes of concomitant regional immune responses.

484 Overall, our data show that systemic inflammation impacts the hosts ability to mount immune
485 responses in LN draining the site of a localized challenge by impairing cell recruitment and
486 restricting tissue remodeling and B cell responses. The prevalence of coinfections in people
487 suggests that it will be important to better define how systemic inflammatory responses in
488 humans impact regional immunity and the progression of diseases that are initiated in barrier
489 tissues.

490

491

492

493 **Methods**

494

495 **Mice.** C57BL/6, B6.SJL-PtprcaPep3b/BoyJ (CD45.1), OBI x B6.129S7-*Rag1*^{tm1Mom}/J
496 (OBI.RAG$^{-/-}$)(Dougan et al., 2012), *Ifnar2*$^{-/-}$, B6.129S2-*Ighm*^{tm1Cgn}/J (μMT$^{-/-}$) and
497 B6.129S4-*Ccr2*^{tm1Ifc}/J (CCR2$^{-/-}$) mice were bred in the Department of Microbiology and
498 Immunology. Animal experiments were approved by The University of Melbourne Animal
499 Ethics Committee. All mice were sex and aged matched and used between 8-14 weeks old at
500 the beginning of experiments.

501

502 **Virus infections.** Mice were infected subcutaneously (s.c.) in the footpad with either 5 x 10^4
503 plaque-forming units (PFU) of HSV-1 (KOS) or 2 x 10^4 PFU of LCMV (Armstrong). Mice
504 were infected intranasally with 10^4 of the recombinant influenza virus X31 expressing the HSV
505 glycoprotein-B-derived epitope $gB_{498–505}$ as described(Davies et al., 2017). For all infections,
506 mice were anaesthetized with isoflurane vaporized in O_2. Unless stated otherwise mice were
507 coinfected intraperitoneally with 2 x 10^5 PFU of LCMV Armstrong two days after footpad
508 HSV infection. HSV-1 viral titers were determined in homogenized footpads by PFU assay as
509 described(Jones et al., 2000).

510

511 **Stromal cell isolation and flow cytometry.** pLN and iLN were harvested and processed as
512 described previously(Gregory et al., 2017). Briefly, LN were teased apart with forceps and
513 incubated at 37°C in RPMI with collagenase D, Dispase and DNase for 25 minutes. Following
514 a second round of digestion for 15 minutes, single cell suspensions were resuspended in FACS
515 buffer (PBS 2% BSA 5mM EDTA) and filtered through 70μM before antibody staining.
516 Antibodies used in this study are listed in Table S1.
517 Live cells were discriminated with a fixable LIVE/DEAD™ Fixable Near-IR Dead Cell Stain
518 Kit (Thermofischer). Annexin V staining was carried out with Annexin V PE and 7AAD from
519 Biolegend according to the manufacturer's instructions.
520 Intracellular staining for KI67 and LCMV were performed using BD Cytofix/Cytoperm™
521 Fixation/Permeabilization Solution Kit according to the manufacturer's instructions. Purified
522 LCMV antibody (Clone VL4, BioXcell) was conjugated to Alexa Fluor™ 594 with antibody
523 labelling kit (ThermoFischer) according to the manufacturer's instructions.
524 Endogenous HSV and LCMV-specific CD8 T cells were identified with H-2Kb-$gB_{498-505}$ and
525 H-2Db-gp_{33-41} (MBL international)-restricted tetramer staining respectively.

526 For metabolism analysis, cells were incubated with Mitotracker Deep Red FM, Bodipy FL C
527 16, CellROX orange reagent or 2-NBDG (all from ThermoFischer) in RPMI supplemented
528 with 10% FCS for 30 minutes at 37°C except for 2-NBDG where glucose-free RPMI
529 (ThermoFischer) was used instead.
530 Cells were enumerated by adding SPHERO calibration particles (BD Biosciences) to each
531 sample before acquisition using FACSCantoII or FACSFortessa (both BD) and Flowjo
532 software was used for analysis.
533
534 **Immunomodulatory treatments.** For $CD8^+$ T cell depletion, mice were injected i.p. twice
535 with 100 µg of anti-CD8 antibody (clone 2.43), 24 hours apart. B cells were depleted with a
536 single injection of 50 µg of anti-mouse CD20 antibody (clone 5D2, Genentech) prior HSV
537 infection. To block lymphocyte egress, FTY720 (2-amino-2-(2-[4-octylphenyl]ethyl)-1,3-
538 propanediol; Cayman chemical, #402616-26-6) was dissolved in 2% cyclodextrin (Sigma) in
539 PBS and i.p. administered daily in mice at a dose of 1mg/kg from day 1 to day 7 post-HSV
540 infection. Control mice were administered with 2% cyclodextrin only. To analyze the effect of
541 systemic inflammation on local immune responses, HSV-infected mice were injected i.p. twice
542 with either 50 µg Polyinosinic:polycytidylic acid high molecular weight (Poly(:IC),
543 InvivoGen) or 5 µg of LPS (Sigma), 24 hours apart. IFNAR in vivo blocking during coinfection
544 was performed by injecting infected mice with 500 µg of anti-IFNAR-1 (clone MAR1-5A3,
545 from BioXcell) or isotype control antibody (clone MOPC-21, BioXcell) for two consecutive
546 days and 250 µg on the third day. Immunization of mice was carried out by injecting 100µg of
547 OVA (Sigma) emulsified in CFA (Sigma) s.c.
548
549 **Lymphocyte recruitment analysis.** C57BL/6-CD45.2 mice were infected s.c. with HSV and
550 two days later injected i.v. with a mixture of 8 million total lymphocytes from pooled LN and
551 spleen from C57BL/6-CD45.1 mice immediately prior to coinfection with LCMV. HSV
552 draining and non-draining LN were analyzed 2 days post LCMV infection.
553
554 **Generation of bone marrow chimeric mice.** To generate IFNAR deficient B cell mice,
555 C57BL/6-Ly5.1 recipient mice were lethally irradiated with two doses of 550 rads, 3 h apart,
556 followed by reconstitution with a 80/20 mixture of 8 x 10^6 $\mu MT^{-/-}$ / WT or $\mu MT^{-/-}$ / *Ifnar2*$^{-/-}$
557 donor bone marrow cells and maintained in antibiotic water (neomycin and polymyxin B) for
558 4 weeks. To analyze the contribution of IFNAR signalling on hematopoietic and non-

559 hematopoietic compartments, C57BL/6-Ly5.2 WT and *Ifnar2*-/- mice were irradiated and
560 reconstituted with either 8 x 106 BM cells from WT or *Ifnar2*-/- donor mice. All recipients
561 were used at least 8 weeks post-reconstitution.
562
563 **Immunofluorescence and confocal microscopy.** Lymph nodes were harvested and fixed in
564 periodate-lysine-paraformaldehyde (PLP) fixative for 4 hours, incubated in 30% sucrose and
565 embedded in OCT freezing media. LN were harvested and immediately embedded in OCT
566 freezing media. Tissue sections were cut at 16 µm thickness with a cryostat (Leica CM3050S)
567 and air-dried before being fixed in acetone for 5 min, dried, and then blocked for 30 min
568 (Protein Block X0909, DAKO) at room temperature (RT). Sections were staining with primary
569 antibodies for 1 hour at RT, washed in PBS and when required stained with secondary
570 antibodies for 45 minutes at RT. Stained sections were mounted in ProLong Gold antifade
571 reagent (Invitrogen), and acquired on a LSM780 or LSM710 confocal microscope (Carl Zeiss)
572 and images processed with Imaris (Bitplane). Antibodies used for histology are listed in Table
573 S1.
574
575 **Detection of HSV-1 IgG by ELISA.** Nunc MaxiSorp round-bottom 96-well ELISA microtiter
576 plates (Thermo Scientific) were coated overnight at 4°C with 10 µg/ml HSV-1 inactivated Vero
577 cell extract (Advanced Biotechnologies). Unbound protein was washed away (PBS 0.05%
578 Tween20) and serially diluted serum samples (PBS 0.5% BSA) were plated and incubated at
579 RT for two hours. Bound mouse IgG Abs were detected using donkey anti-mouse IgG-HRP
580 and visualized using o-Phenylenediamine. The OD readings were determined at 450/492 nm.
581 Endpoint titers of anti-HSV-1 were calculated by using cut-off values defined as double the
582 OD of non-infected serum control.
583
584 **Statistical analysis.** Graphs and statistics were generated using Prism 8 (GraphPad). Samples
585 were tested for normality and two groups were compared using two-tailed Mann-Whitney U-
586 test or unpaired t-test. Multiple groups were analyzed with one-way Anova followed by
587 Tukey's post-test comparison or Kruskal-Wallis, based on Gaussian distribution. All graphs
588 depict means ± SEM.
589
590

591 **Table S1.** Antibodies used for immunofluorescence staining, flow cytometry, blocking and
592 depletion experiments.

Antibody	Clone	Supplier	Application	Fluorochrome
anti-Hamster	Polyclonal	Invitrogen	IF	A647
anti-Rabbit IgG	Polyclonal	Invitrogen	IF	A488
anti-Rabbit IgG	Polyclonal	Invitrogen	IF	A594
anti-Rat IgG	Polyclonal	Invitrogen	IF	A594
B220	RA3-6B2	Biolegend	IF	Pacific Blue
B220	RA3-6B2	Biolegend	FC	PE-Cy7
B220	RA3-6B2	Biolegend	FC	A700
CD138	281-2	BD	FC	PE
CD138	281-2	Biolegend	IF	A647
CD157	BP-3	Biolegend	FC	APC
CD157	BP-3	BD OptiBuild	FC	BV650
CD19	1D3	BD	FC	PerCP/Cy5.5
CD19	1D3	BD	FC	BV605
CD20	5D2	Genentech	depletion	purified
CD31	390	Biolegend	FC	BV421
CD31	MEC13.3	BD	FC	PE
CD31	MEC13.3	Biolegend	IF	A647
CD31	390	ThermoFisher	FC	FITC
CD31	390	Biolegend	FC	Pe-Cy7
CD38	90	Biolegend	FC	PE-Cy7
CD3e	eBio500A2	ThermoFisher	FC	A700
CD4	RM4-5	Biolegend	FC	BV605
CD4	RM4-5	BD	FC	PE-Cy7
CD4	RM4-5	BD	FC	APC
CD45	l3/2.3	Biolegend	FC	A700
CD45	30-F11	BD	FC	PerCP
CD45.2	104	BD	FC	A700
CD8a	2.43	Bio X Cell	depletion	purified
CD8a	53-6.7	Biolegend	FC	BV785
CD8a	53-6.7	Biolegend	FC	APC
CD8b	eBioH35-17.2	ThermoFisher	FC	APC
CD8b	YTS156.7.7	Biolegend	FC	A700
CD8b	H35-17.2	BD	FC	BV785
CXCR5	SPRCL5	ThermoFisher	FC	Biotin
FDCM2	FDC-M2	ImmunoKontact	FC	purified
GL7	GL7	Biolegend	FC	A647
GL7	GL7	Biolegend	IF	Pacific Blue
IFNAR-1	MAR1-5A3	Bio X Cell	blocking	purified
IgD	11-26c.2a	Biolegend	IF	A594
IgG1 isotype control	MOPC-21	Bio X Cell	blocking	purified
KI-67	SolA15	ThermoFisher	FC	eFluor660
Laminin	polyclonal	Abcam	IF	purified
LCMV	VL4	Bio X Cell	FC	purified

Lyve1	polyclonal	Abcam	IF	purified
MAdCAM-1	MECA-367	Biolegend	FC	Biotin
MAdCAM-1	MECA-367	Biolegend	IF	purified
PD1	29F.1A12	Biolegend	FC	PerCP/C5.5
PNAd	MECA-79	ThermoFisher	FC, IF	A488
podoplanin	8.1.1	ThermoFisher	FC	PE
podoplanin	8.1.1	Biolegend	FC	PE-Cy7
podoplanin	8.1.1	Biolegend	IF	purified
podoplanin	8.1.1	ThermoFisher	FC	A488
RANK-L	IK22/5	ThermoFisher	FC	Biotin
Streptavidin		Life Technologies	IF	A555
Streptavidin		BD	FC	APC
Streptavidin		BD	FC	FITC
Streptavidin		BD	FC	PE
Streptavidin		Biolegend	FC	BV711
Streptavidin		BD	FC	PE-Cy7
TCRb	H57-597	BD	FC	BV711
TCRb	H57-597	BD	FC	FITC
TER-119	TER-119	ThermoFisher	FC	PerCP.Cy5.5
TER-119	TER-119	Biolegend	FC	A700

IF, immunofluorescence; FC, flow cytometry

Acknowledgments

We thank Paul Hertzog (Hudson Institute, Australia) for anti-IFNAR antibody, Hidde Ploegh (Whitehead Institute, Cambridge, MA) for OBI mice, Genentech for anti-mouse CD20 antibody, the Biological Optical Microscopy Platform (BOMP) for support, and Yu Kato for advice on HSV ELISA.

Funding: This work was supported by the National Health and Medical Research Council of Australia and the Australian Research Council (to LKM, WRH and SNM).

Author contributions: Conceptualization, YOA and SNM; Methodology, YOA and SD; Investigation, YOA, SD, and SLP; Writing, YOA and SNM; Resources, PJH, LKM and WRH; Visualization, YOA and SNM; Funding acquisition, SNM.

Competing interests: The authors declare no competing interests.

609 **References**

610

611 Alexandre, Y.O., and Mueller, S.N. (2018). Stromal cell networks coordinate immune response
612 generation and maintenance. Immunol Rev *283*, 77-85.
613 Angeli, V., Ginhoux, F., Llodra, J., Quemeneur, L., Frenette, P.S., Skobe, M., Jessberger, R.,
614 Merad, M., and Randolph, G.J. (2006). B cell-driven lymphangiogenesis in inflamed lymph
615 nodes enhances dendritic cell mobilization. Immunity *24*, 203-215.
616 Barton, E.S., White, D.W., Cathelyn, J.S., Brett-McClellan, K.A., Engle, M., Diamond, M.S.,
617 Miller, V.L., and Virgin, H.W.t. (2007). Herpesvirus latency confers symbiotic protection from
618 bacterial infection. Nature *447*, 326-329.
619 Chang, C.C., Crane, M., Zhou, J., Mina, M., Post, J.J., Cameron, B.A., Lloyd, A.R., Jaworowski,
620 A., French, M.A., and Lewin, S.R. (2013). HIV and co-infections. Immunol Rev *254*, 114-142.
621 Cremasco, V., Woodruff, M.C., Onder, L., Cupovic, J., Nieves-Bonilla, J.M., Schildberg, F.A.,
622 Chang, J., Cremasco, F., Harvey, C.J., Wucherpfennig, K.*, et al.* (2014). B cell homeostasis and
623 follicle confines are governed by fibroblastic reticular cells. Nat Immunol *15*, 973-981.
624 Cyster, J.G., and Allen, C.D.C. (2019). B Cell Responses: Cell Interaction Dynamics and
625 Decisions. Cell *177*, 524-540.
626 Davies, B., Prier, J.E., Jones, C.M., Gebhardt, T., Carbone, F.R., and Mackay, L.K. (2017). Cutting
627 Edge: Tissue-Resident Memory T Cells Generated by Multiple Immunizations or Localized
628 Deposition Provide Enhanced Immunity. J Immunol *198*, 2233-2237.
629 Denton, A.E., Roberts, E.W., Linterman, M.A., and Fearon, D.T. (2014). Fibroblastic reticular
630 cells of the lymph node are required for retention of resting but not activated CD8+ T cells.
631 Proc Natl Acad Sci U S A *111*, 12139-12144.
632 Dougan, S.K., Ogata, S., Hu, C.C., Grotenbreg, G.M., Guillen, E., Jaenisch, R., and Ploegh, H.L.
633 (2012). IgG1+ ovalbumin-specific B-cell transnuclear mice show class switch recombination in
634 rare allelically included B cells. Proc Natl Acad Sci U S A *109*, 13739-13744.
635 Doughty, L., Nguyen, K., Durbin, J., and Biron, C. (2001). A role for IFN-alpha beta in virus
636 infection-induced sensitization to endotoxin. J Immunol *166*, 2658-2664.
637 Edwards, C.L., Zhang, V., Werder, R.B., Best, S.E., Sebina, I., James, K.R., Faleiro, R.J., de
638 Labastida Rivera, F., Amante, F.H., Engwerda, C.R.*, et al.* (2015). Coinfection with Blood-Stage
639 Plasmodium Promotes Systemic Type I Interferon Production during Pneumovirus Infection
640 but Impairs Inflammation and Viral Control in the Lung. Clin Vaccine Immunol *22*, 477-483.
641 Fallet, B., Narr, K., Ertuna, Y.I., Remy, M., Sommerstein, R., Cornille, K., Kreutzfeldt, M., Page,
642 N., Zimmer, G., Geier, F.*, et al.* (2016). Interferon-driven deletion of antiviral B cells at the
643 onset of chronic infection. Sci Immunol *1*.
644 Gregory, J.L., Walter, A., Alexandre, Y.O., Hor, J.L., Liu, R., Ma, J.Z., Devi, S., Tokuda, N., Owada,
645 Y., Mackay, L.K.*, et al.* (2017). Infection Programs Sustained Lymphoid Stromal Cell Responses
646 and Shapes Lymph Node Remodeling upon Secondary Challenge. Cell Rep *18*, 406-418.
647 Griffiths, E.C., Pedersen, A.B., Fenton, A., and Petchey, O.L. (2011). The nature and
648 consequences of coinfection in humans. J Infect *63*, 200-206.
649 Halin, C., Scimone, M.L., Bonasio, R., Gauguet, J.M., Mempel, T.R., Quackenbush, E., Proia,
650 R.L., Mandala, S., and von Andrian, U.H. (2005). The S1P-analog FTY720 differentially
651 modulates T-cell homing via HEV: T-cell-expressed S1P1 amplifies integrin activation in
652 peripheral lymph nodes but not in Peyer patches. Blood *106*, 1314-1322.

653 Hastey, C.J., Ochoa, J., Olsen, K.J., Barthold, S.W., and Baumgarth, N. (2014). MyD88- and
654 TRIF-independent induction of type I interferon drives naive B cell accumulation but not loss
655 of lymph node architecture in Lyme disease. Infect Immun *82*, 1548-1558.
656 Hor, J.L., Whitney, P.G., Zaid, A., Brooks, A.G., Heath, W.R., and Mueller, S.N. (2015).
657 Spatiotemporally Distinct Interactions with Dendritic Cell Subsets Facilitates CD4+ and CD8+
658 T Cell Activation to Localized Viral Infection. Immunity *43*, 554-565.
659 Hotchkiss, R.S., Monneret, G., and Payen, D. (2013). Sepsis-induced immunosuppression:
660 from cellular dysfunctions to immunotherapy. Nat Rev Immunol *13*, 862-874.
661 Huang, H.Y., Rivas-Caicedo, A., Renevey, F., Cannelle, H., Peranzoni, E., Scarpellino, L., Hardie,
662 D.L., Pommier, A., Schaeuble, K., Favre, S.*, et al.* (2018). Identification of a new subset of
663 lymph node stromal cells involved in regulating plasma cell homeostasis. Proc Natl Acad Sci U
664 S A *115*, E6826-E6835.
665 Jones, C.M., Cose, S.C., Coles, R.M., Winterhalter, A.C., Brooks, A.G., Heath, W.R., and
666 Carbone, F.R. (2000). Herpes simplex virus type 1-specific cytotoxic T-lymphocyte arming
667 occurs within lymph nodes draining the site of cutaneous infection. J Virol *74*, 2414-2419.
668 Kamphuis, E., Junt, T., Waibler, Z., Forster, R., and Kalinke, U. (2006). Type I interferons
669 directly regulate lymphocyte recirculation and cause transient blood lymphopenia. Blood *108*,
670 3253-3261.
671 Kenney, L.L., Cornberg, M., Chen, A.T., Emonet, S., de la Torre, J.C., and Selin, L.K. (2015).
672 Increased Immune Response Variability during Simultaneous Viral Coinfection Leads to
673 Unpredictability in CD8 T Cell Immunity and Pathogenesis. J Virol *89*, 10786-10801.
674 Kuka, M., and Iannacone, M. (2018). Viral subversion of B cell responses within secondary
675 lymphoid organs. Nat Rev Immunol *18*, 255-265.
676 Kumar, V., Scandella, E., Danuser, R., Onder, L., Nitschke, M., Fukui, Y., Halin, C., Ludewig, B.,
677 and Stein, J.V. (2010). Global lymphoid tissue remodeling during a viral infection is
678 orchestrated by a B cell-lymphotoxin-dependent pathway. Blood *115*, 4725-4733.
679 Langhorne, P., Stott, D.J., Robertson, L., MacDonald, J., Jones, L., McAlpine, C., Dick, F., Taylor,
680 G.S., and Murray, G. (2000). Medical complications after stroke: a multicenter study. Stroke
681 *31*, 1223-1229.
682 Mabbott, N.A. (2018). The Influence of Parasite Infections on Host Immunity to Co-infection
683 With Other Pathogens. Front Immunol *9*, 2579.
684 Malhotra, D., Fletcher, A.L., Astarita, J., Lukacs-Kornek, V., Tayalia, P., Gonzalez, S.F., Elpek,
685 K.G., Chang, S.K., Knoblich, K., Hemler, M.E.*, et al.* (2012). Transcriptional profiling of stroma
686 from inflamed and resting lymph nodes defines immunological hallmarks. Nat Immunol *13*,
687 499-510.
688 McAfee, M.S., Huynh, T.P., Johnson, J.L., Jacobs, B.L., and Blattman, J.N. (2015). Interaction
689 between unrelated viruses during in vivo co-infection to limit pathology and immunity.
690 Virology *484*, 153-162.
691 Moseman, E.A., Wu, T., de la Torre, J.C., Schwartzberg, P.L., and McGavern, D.B. (2016). Type
692 I interferon suppresses virus-specific B cell responses by modulating CD8(+) T cell
693 differentiation. Sci Immunol *1*.
694 Mueller, S.N., and Germain, R.N. (2009). Stromal cell contributions to the homeostasis and
695 functionality of the immune system. Nat Rev Immunol *9*, 618-629.
696 Mueller, S.N., Hosiawa-Meagher, K.A., Konieczny, B.T., Sullivan, B.M., Bachmann, M.F.,
697 Locksley, R.M., Ahmed, R., and Matloubian, M. (2007a). Regulation of homeostatic
698 chemokine expression and cell trafficking during immune responses. Science *317*, 670-674.

699 Mueller, S.N., Matloubian, M., Clemens, D.M., Sharpe, A.H., Freeman, G.J., Gangappa, S.,
700 Larsen, C.P., and Ahmed, R. (2007b). Viral targeting of fibroblastic reticular cells contributes
701 to immunosuppression and persistence during chronic infection. Proc Natl Acad Sci U S A *104*,
702 15430-15435.
703 Nansen, A., and Randrup Thomsen, A. (2001). Viral infection causes rapid sensitization to
704 lipopolysaccharide: central role of IFN-alpha beta. J Immunol *166*, 982-988.
705 Olson, M.R., McDermott, D.S., and Varga, S.M. (2012). The initial draining lymph node primes
706 the bulk of the CD8 T cell response and influences memory T cell trafficking after a systemic
707 viral infection. PLoS Pathog *8*, e1003054.
708 Sammicheli, S., Kuka, M., Di Lucia, P., de Oya, N.J., De Giovanni, M., Fioravanti, J., Cristofani,
709 C., Maganuco, C.G., Fallet, B., Ganzer, L.*, et al.* (2016). Inflammatory monocytes hinder
710 antiviral B cell responses. Sci Immunol *1*.
711 Stelekati, E., and Wherry, E.J. (2012). Chronic bystander infections and immunity to unrelated
712 antigens. Cell Host Microbe *12*, 458-469.
713 Straub, T., Freudenberg, M.A., Schleicher, U., Bogdan, C., Gasteiger, G., and Pircher, H. (2018).
714 Bacterial coinfection restrains antiviral CD8 T-cell response via LPS-induced inhibitory NK
715 cells. Nat Commun *9*, 4117.
716 Wu, Y., Tu, W., Lam, K.T., Chow, K.H., Ho, P.L., Guan, Y., Peiris, J.S., and Lau, Y.L. (2015). Lethal
717 coinfection of influenza virus and Streptococcus pneumoniae lowers antibody response to
718 influenza virus in lung and reduces numbers of germinal center B cells, T follicular helper cells,
719 and plasma cells in mediastinal lymph Node. J Virol *89*, 2013-2023.
720 Yager, E.J., Szaba, F.M., Kummer, L.W., Lanzer, K.G., Burkum, C.E., Smiley, S.T., and Blackman,
721 M.A. (2009). gamma-Herpesvirus-induced protection against bacterial infection is transient.
722 Viral Immunol *22*, 67-72.
723 Yang, C.Y., Vogt, T.K., Favre, S., Scarpellino, L., Huang, H.Y., Tacchini-Cottier, F., and Luther,
724 S.A. (2014). Trapping of naive lymphocytes triggers rapid growth and remodeling of the
725 fibroblast network in reactive murine lymph nodes. Proc Natl Acad Sci U S A *111*, E109-118.
726

727

728 **Supplemental Figures**

729

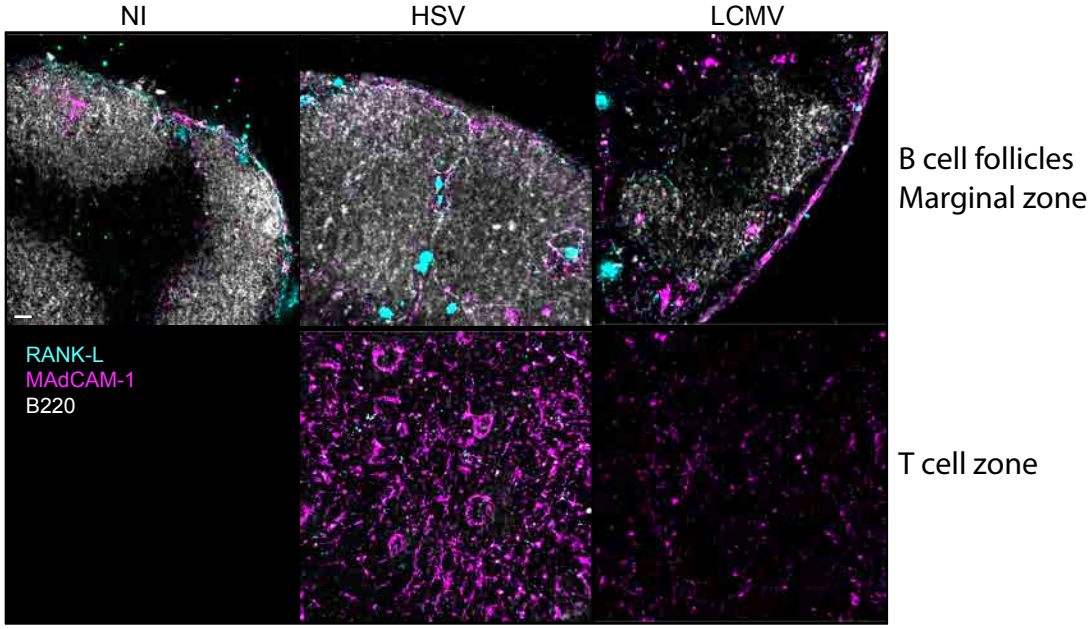

730
731 **Fig. S1. FRC upregulate MAdCAM-1 expression during HSV infection.** pLN sections from
732 NI, HSV or LCMV infected mice were stained for B220, RANK-L and MAdCAM-1, and
733 analyzed by confocal microscopy. Data are representative of 2 experiments with 3 mice per
734 group. Scale bar, 40μm.
735
736

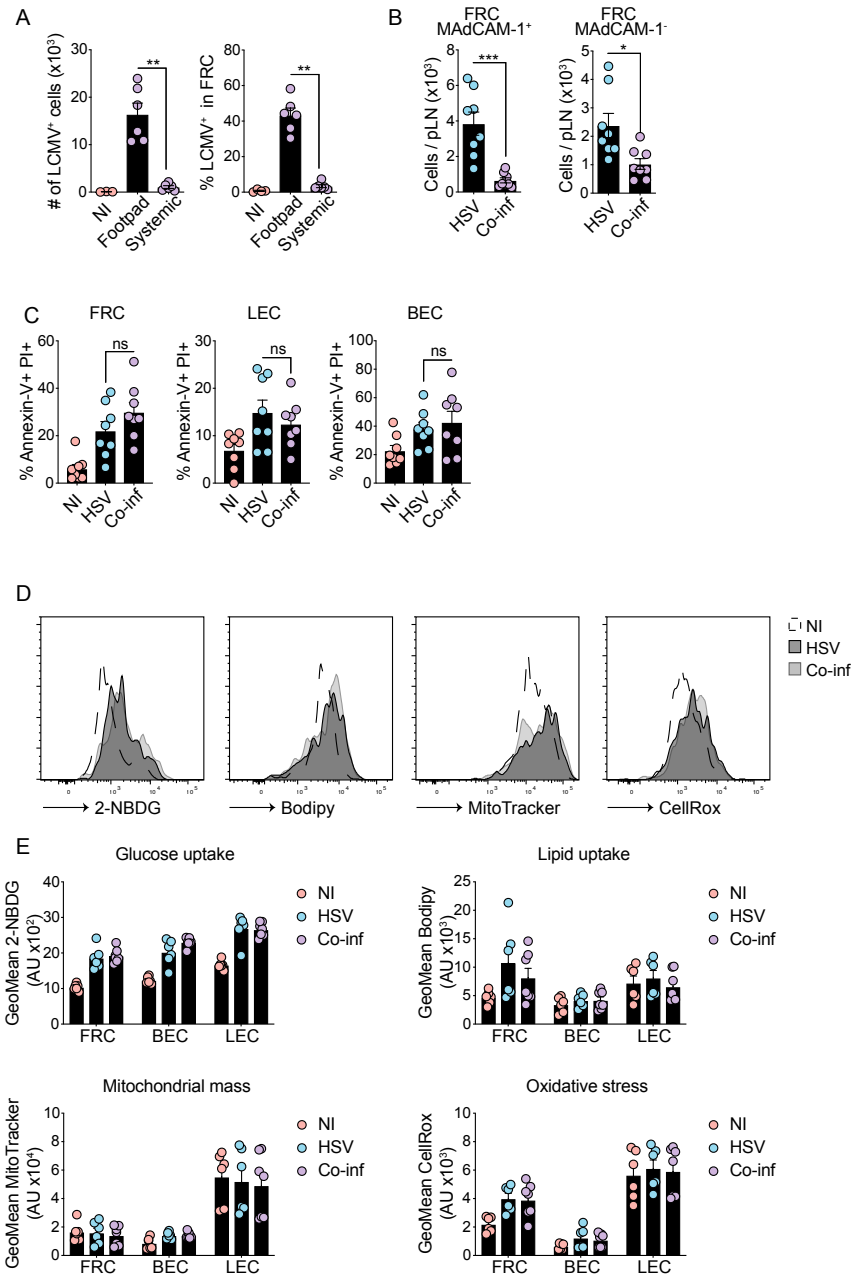

Fig. S2. Systemic coinfection impairs stromal cell expansion. (A) Mice were infected with LCMV s.c. or i.p. and pLN harvested 3 d post-infection. LCMV was detected by intracellular staining and analyzed by flow cytometry. Left graph displays total LCMV infected cells, right graph the percentage of infected FRC. Graphs show pooled data (mean ± SEM) from 2 independent experiments with 3 mice per group. **P < 0.01, by Mann-Whitney test (B) Mice were infected with HSV or coinfected as described in Fig. 3. Numbers of FRC expressing or not MAdCAM-1 in pLN were analyzed by flow cytometry. Graphs show pooled data (mean ± SEM) from 2 independent experiments with 4 mice per group. *P < 0.05, *** P < 0.001, by unpaired two-tailed t test. (C) pLN from HSV and coinfected mice were harvested 5 d post-infection and analyzed for Annexin V and PI expression on stromal cells by flow cytometry. iLN from naïve mice were included as controls. Graphs show pooled data (mean ± SEM) from 2 independent experiments with 4 mice per group. ns, non-significant, by by unpaired two-tailed t test (D-E) Metabolism of stromal cells during infection. Mice were infected as in Fig. 3 and pLN harvested 8 days post-infection. iLN from naïve mice were used as controls. Cells were incubated with the fluorescent glucose analog 2-NBDG, the fluorescent fatty acid analog

BODIPY FL C16, Mitotracker or CellRox before analysis by flow cytometry. Representative histograms on FRC (D) and analysis of geometric mean values on stromal cell subsets (E). Graphs show pooled data (mean ± SEM) from two independent experiments with 3-4 mice per group.

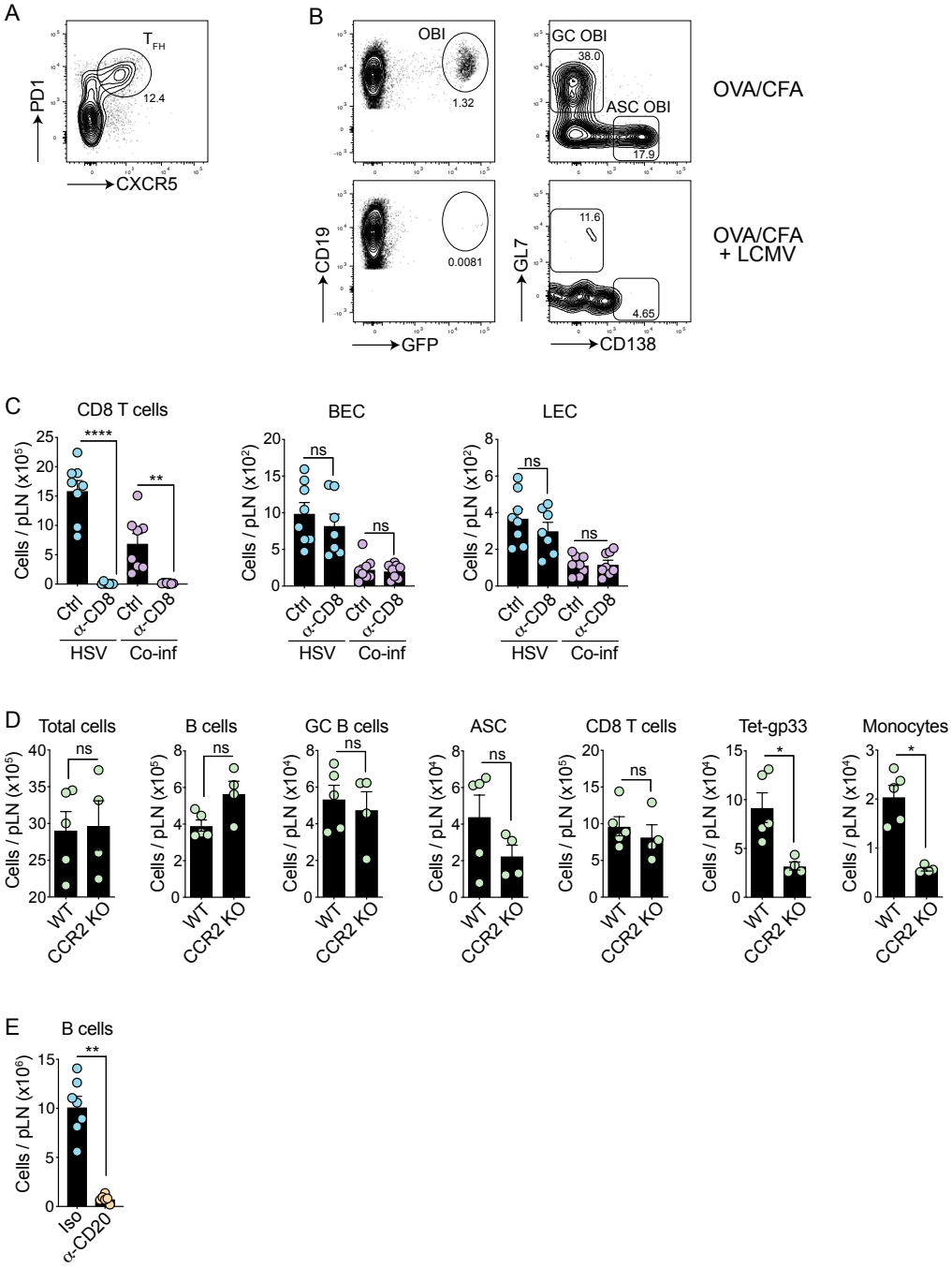

Fig. S3. Lymphopenia suppresses LN expansion and B cell responses.
(A) Gating strategy to identify T_{FH} in infected mice. $CD4^+$ T cells were analyzed for CXCR5 and PD1 expression and TFH cells defined as $CD4^+$ $CXCR5^+$ $PD1^+$ cells. (B) OBI B cell response in the pLN. Mice were injected i.v. with transgenic OBI-GFP cells and two days later injected s.c. with an emulsion of OVA/CFA. Mice were infected i.p. with LCMV 2 d post immunisation and pLN harvested 8 d post OVA/CFA injection. Gating strategy to identify OBI cells in the pLN. $CD19^+$ $CD3\varepsilon^-$ B cells were analyzed for GFP expression and OBI cells

767 analyzed for GL7 and CD138 expression to identify GC OBI and ASC OBI. (C) Experimental
768 procedure as in Fig. 5A. Absolute numbers of $CD8^+$ T cells BEC and LEC in the pLN of mice
769 infected with HSV or coinfected with or without $CD8^+$ T cells. Graphs show pooled data (mean
770 ± SEM) from 2 independent experiments with 3-4 mice per group. **P < 0.01, ****P < 0.0001,
771 ns, non-significant, by ANOVA with Krukal-Wallis test (D) Monocytes are not required for
772 $CD8^+$ and B cell responses during LCMV infection. WT and CCR2 KO mice were infected
773 with LCMV s.c. and pLN harvested 8 d post-infection. B cell and T cell responses were
774 analyzed by flow cytometry. Graphs show data from 1 representative experiment out of 2
775 (mean ± SEM) with 4-5 mice per group. (E) B cell depletion following CD20 antibody
776 depleting antibody injection. See Fig. 5F for experimental procedure. *P < 0.05, **P < 0.01,
777 ns, non-significant, by Mann-Whitney test.
778
779
780

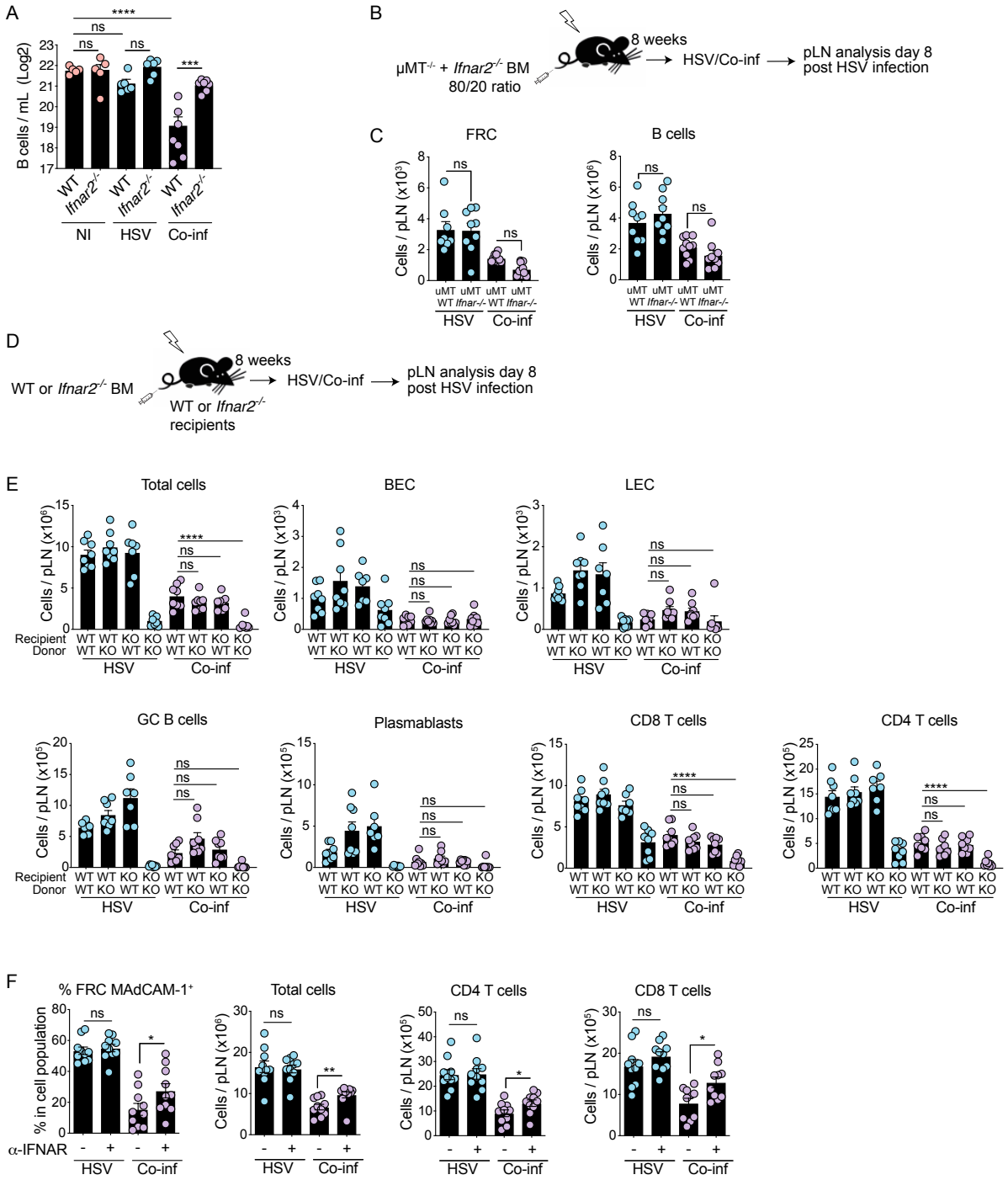

Fig. S4. IFN-I induces local LN suppression via B cell-extrinsic IFNAR signals. (A) B cell cellularity in the blood of infected mice. WT or *Ifnar2*$^{-/-}$ mice were infected with HSV s.c. and the following day infected with LCMV i.p. Blood was collected on day 3 and B cell numbers analyzed by flow cytometry. Graph shows pooled data (mean ± SEM) from 2 independent experiments with 2-4 mice per group. **P < 0.01, *** P < 0.001, ****P < 0.0001, ns, non-significant, by ANOVA with Dunnett's multiple comparisons test. (B) Experimental schematic of generating IFNAR deficient B cells. Lethally irradiated mice received a mixture of 80/20 bone marrow cells from μMT + *Ifnar2* or μMT + WT donor mice. 8 weeks post reconstitution, mice were HSV and coinfected as described in Fig. 3A. (C) Absolute numbers of FRC and B cells in the pLN of HSV and coinfected mice in IFNAR B cell deficient mice. Graphs show pooled data (mean ± SEM) from two independent experiments with 4-5 mice per group. *P < 0.05, **P < 0.01, ***P < 0.001, ns, non-significant, by ANOVA with Kruskal-Wallis test. (D)

794 Experimental schematic of generating IFNAR BM chimeras. Lethally irradiated WT or *Ifnar2*-
795 /- recipient mice received BM cells from WT or *Ifnar2*-/- donor mice. 8 weeks post
796 reconstitution, mice were HSV and coinfected. (E) Cell numbers in the pLN of HSV and
797 coinfected mice. Graphs show pooled data (mean ± SEM) from two independent experiments.
798 *P < 0.05, **P < 0.01, ***P < 0.001, ns, non-significant, by ANOVA with Kruskal-Wallis test.
799 (F) Mice were infected as in Fig. 6D. Analysis of cellularity of total cells, HEV, $CD4^+$ and
800 $CD8^+$ T cells in the pLN of HSV and coinfected mice during IFNAR blocking. Graphs show
801 pooled data (mean ± SEM) from 2 independent experiments with 5 mice per group. *P < 0.05,
802 **P < 0.01, ***P < 0.001, ns, non-significant, by unpaired t test.
803